Amorphization induced by subnanosecond laser pulses in phase-change optical recording media

Chubing Peng and Masud Mansuripur

We have investigated the dynamics of amorphization induced in phase-change optical recording media by focused laser pulses of subnanosecond duration. We initiated localized amorphism by using a focused laser beam to melt the phase-change material and completed the change by rapid cooling by means of thermal diffusion. These studies were conducted by use of real-time reflectivity measurements with a pump-and-probe technique in which both pump and probe pulses had a duration of ~510 ps. Our transient-reflectivity measurements indicate that the process that leads to amorphism has three distinct stages, namely, rapid melting, solidification, and slow relaxation. © 2004 Optical Society of America

OCIS codes: 210.0210, 210.4810.

1. Introduction

In erasable phase-change (PC) optical disk data storage, one writes a bit of information by applying a short pulse of a focused laser beam to a crystallized area of the disk.[1–5] This pulse increases the local temperature of the storage layer above its melting point. When the pulse ends, the molten spot cools rapidly and subsequently amorphizes. The recorded mark can later be identified by use of the same focused laser beam (at a much lower incident power) to measure the reflection of the spot relative to its crystalline surroundings. Erasure is achieved by exposure of the film to intermediate levels of laser power for a sufficient length of time, raising the local temperature of the storage layer above its glass transition point (but below its melting temperature). The amorphous mark thus recrystallizes while the surrounding crystalline matrix remains largely unaffected; optical contrast between the mark and its surroundings is thereby eliminated.

The data-transfer rate that is achievable with rewritable PC media is determined primarily by the duration of time needed to recrystallize an amorphous mark. To achieve high data rates, one would prefer storage materials that have fast crystallization mechanisms. If the storage layer is embedded in a multilayer stack with a relatively slow cooling rate (to aid recrystallization), then amorphism will become critical because of the possibility of partial crystallization during quenching from the melt. Such partial crystallization decreases the optical contrast between amorphous marks and their crystalline surroundings. It also produces relatively large, irregular crystallites about the periphery of amorphous marks. These undesirable crystallites scatter light and produce high levels of noise and jitter during readout.[6]

A conventional rewritable PC optical disk typically consists of a substrate, two dielectric layers surrounding a PC layer, and a heat-sinking metallic layer to cap off the stack. The thickness of each layer in this quadrilayer is generally optimized for good optical contrast during readout, but it is also designed to produce a reasonable cooling rate for amorphization. To increase the cooling rate, one can reduce the thickness of the dielectric film between the storage layer and the heat-sinking layer, increase the thickness of the heat-sinking layer, or use a thinner storage layer. Under such circumstances, because the heat generated within the storage layer is rapidly diffused away and is absorbed by the heat-sinking layer, a large amount of optical energy is needed for the sample to reach the high temperatures required for melting.

An effective way to deliver laser energy to rapidly cooling media is by means of short pulses. If the pulse duration happens to be shorter than the characteristic diffusion time within the storage layer, the

When this research was conducted, the authors were with the Optical Sciences Center, University of Arizona, Tucson, Arizona 85721. C. Peng (chubing.peng@seagate.com) is now with Seagate Research, Pittsburgh, Pennsylvania 15222.

Received 6 February 2004; revised manuscript received 11 May 2004; accepted 18 May 2004.

0003-6935/04/224367-09$15.00/0

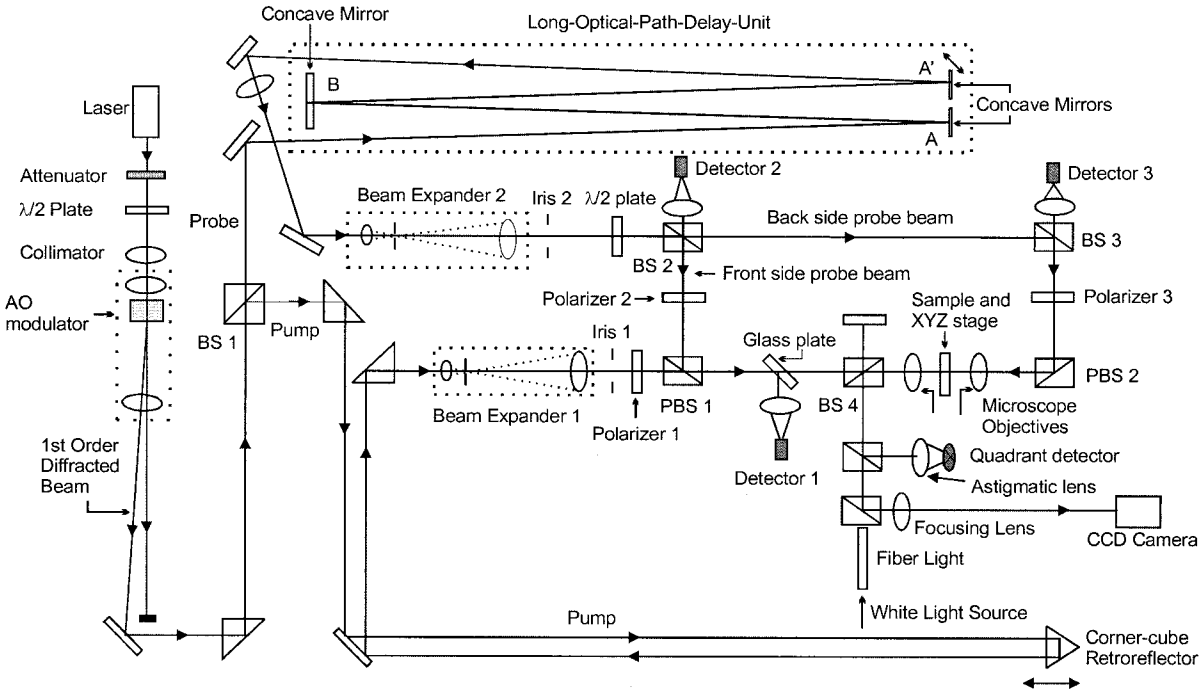

Fig. 1. Schematic diagram of the pump-and-probe tester used in our experiments. A laser beam, gated by an AO modulator, is split into pump and probe beams by beam splitter BS 1. After being delayed (by going through variable-length paths), the pump and the parallel probe beams are combined at polarizing beam splitter PBS 1 and then focused onto the sample by an objective lens. The optical path length of the probe beam can be changed in multiples of 3.2 m in the LOPD unit. The path length of the pump beam can be adjusted within a 3-m range (round trip) with the resolution of the translation stage. The parallel probe beam reflected from (transmitted through) the sample is detected by Detector 2 (3). The parallel probe is blocked whenever the antiparallel probe is used to examine the sample from its rear side (as opposed to the front side, which is the side illuminated by the pump beam). The antiparallel probe reflected from the rear of the sample is monitored by Detector 3. Other abbreviations are defined in text.

entire energy content of the pulse will be absorbed locally, thus raising the temperature of the medium to its highest possible value for the given amount of optical energy. Moreover, the large thermal gradients thus established quickly remove the heat from the hot spot, giving rise to cooling rates above and beyond what is possible with longer pulses.

It has been shown that reversible amorphization and crystallization can be induced with femtosecond and picosecond laser pulses in fast-crystallizing materials such as GeSb films.[7,8] The application of femtosecond and picosecond laser pulses in optical storage is limited by the nature of the lasers themselves, which, in general, not only have been large, inefficient, and expensive but also have required a high level of care to maintain their performance.

In this paper we investigate the application of subnanosecond laser pulses to induce phase transitions in the media of phase-change optical recording. Subnanosecond laser pulses can be obtained by compression of pulses of a few-nanosecond's duration or by use of a diode-pumped, passively Q-switched solid-state laser, the so-called nanolaser. Commercially available nanolasers produce high-intensity, linearly polarized laser light with good beam quality in a range of wavelengths from the infrared to the ultraviolet and can be obtained at reasonable prices these days. The readily available pulse duration from these lasers is typically a few hundred picoseconds, obtained at a repetition rate of several kilohertz. Using a pump-and-probe technique in which both the pump and the probe pulses are ~0.5 ns long, we have investigated the time-resolved dynamics of amorphization in a few samples of phase-change recording media.

2. Time-Resolved Pump-and-Probe Tester

To explore the dynamics of amorphization induced by subnanosecond laser pulses we measure the reflectivity or transmissivity transients or both of a sample, using a pump-and-probe tester. Figure 1 is a schematic diagram of our tester. A nanolaser operating at $\lambda = 532$ nm is used as a light source; it has pulse duration $\tau = 510$ ps at a repetition rate of 5.7 kHz, and the energy contained in each pulse is $E = 4.7$ μJ. The laser beam is first attenuated (by a neutral-density filter) and then collimated. Between the attenuator and the collimator, a half-wave ($\lambda/2$) plate is inserted to rotate the polarization vector of the beam to the p direction, which is the preferred polarization for the acousto-optic (AO) modulator. The beam is subsequently focused onto an AO crystal and recollimated afterward. The first-order diffracted beam out of the AO modulator is used in our experiments, whereas the zero-order beam is blocked. The modulator thus isolates single pulses from the

periodic train of pulses by diverting them, on command, into the main optical path of the pump-and-probe tester; it also controls the intensity of the first-order diffracted beam.

After reflection from a turning mirror and a prism, the beam is divided at the first beam splitter (BS 1) into a pump beam and a probe beam. The probe beam is sent through a long-optical-path delay (LOPD) unit that is capable of variable delay. This device is essentially a system of conjugate foci consisting of three concave spherical mirrors (A, A′, and B in Fig. 1), all of which have the same radius of curvature.[9] The centers of curvature of mirrors A and A′ are on the front surface of mirror B, and the center of curvature of mirror B is halfway between A and A′. The light leaving mirror A (A′) is brought to focus by mirror B at a conjugate point on mirror A′ (A). Similarly, the light that leaves mirror B is focused back onto B at a new location that is somewhat offset from its point of origin. The number of times that the light travels back and forth in the unit is determined by the ratio of the diameter of mirror B to the distance between the curvature centers of mirrors A and A′; one can change the latter simply by tilting mirror A′. In our system the probe beam's optical path length can be made to vary from 3.2 to 22.4 m in steps of 3.2 m by use of this LOPD unit.

The optical path length of the pump beam is also adjustable with a corner-cube mirror mounted upon a translation stage, which serves to fine tune the relative delay between the pump and the probe beams. In our experiments the probe beam's path length is fixed, and the translation of the retroreflector is used to adjust the delay of the probe pulse relative to the pump pulse. A stage motion of 1.5 m (3-m round trip) produces a 10-ns delay, with a resolution determined solely by the fine translation steps taken by the retroreflector.

On exiting the LOPD unit, the probe is expanded by Beam Expander 2 (Fig. 1). A pinhole at the common focal plane of the expander performs spatial filtering on the probe beam. The combination of Expander 2 and Iris 2 minimizes the effects of beam displacement caused by air turbulence, mechanical vibrations of the LOPD mirrors, etc. The probe beam then goes through another $\lambda/2$ plate and is divided into two parts by another beam splitter, BS 2. The $\lambda/2$ plate is mounted upon a rotary stage driven by a stepper motor, thus facilitating control of the probe beam's intensity. (To minimize the thermal effects of the probe on the sample, we typically set the probe's power to a small fraction of the pump power.)

Splitting the probe at BS 2 yields two probe pulses for monitoring both sides of the sample. The sample can thus be probed either from its film side or through its substrate, although the two measurements cannot be made simultaneously. In what follows, parallel probing will refer to the situation when the pump and the probe illuminate the same side of the sample, whereas antiparallel probing will signify that the pump and the probe arrive from opposite sides of the sample. Each probe beam passes through a polarizer (Polarizers 2 and 3 in Fig. 1), which sets the direction of polarization of the probe perpendicular to the plane of the diagram. Because the pump beam is linearly polarized in the plane of the diagram, polarizers 2 and 3 help to reduce the amount of scattered pump light that reaches the detectors (Detectors 2 and 3 in Fig. 1).

After reflection from the corner-cube retroreflector, the pump beam is expanded and spatially filtered by Beam Expander 1. This expander reduces the possibility of varying overlap between pump and probe at the sample as a result of the motion of the corner cube. Ideally, the pump beam directed toward the corner cube is parallel to the direction of translation of the stage. If perfect alignment is achieved, the beam returning from the corner cube will not shift laterally, nor will it change its propagation direction, with any translation of the stage. Misalignment, however, can cause lateral beam displacement as a function of the corner-cube's position. Moreover, if the mount is somehow warped, the orientation of the retroreflector can change as the corner cube is moved; this will also change the direction of the pump beam. The combination of Beam Expander 1 and Iris 1 mitigates the lateral shift of the focused pump beam at the sample. Diffraction, misalignment, or both cause the beam intensity exiting Iris 1 to vary as the corner cube is translated; a 5% change in the pump power has been observed experimentally. To keep the pump power constant at the sample, we place Polarizer 1 in the beam's path (after Iris 1). Rotating this polarizer keeps the power of the pump beam at the sample at a constant value.

The pump and the parallel probe are combined at a polarizing beam splitter (PBS 1) and then focused by a 0.4-N.A. microscope objective onto the sample, which is mounted onto an *XYZ* positioner. For calibration purposes, a flat glass plate mounted at 45° to the optical axis is used to direct a fraction of the light to Detector 1. The probe beam reflected from (transmitted through) the sample is captured by Detector 2 (3).

In antiparallel probing, the back-side probe is directed by a beam splitter, BS3, and a polarizing beam splitter, PBS 2, toward the sample, and then focused onto the sample by a 0.6-NA microscope objective. The reflected probe from the back side of the sample is detected at Detector 3. Both Detectors 2 and 3 have bandwidths of ~200 MHz, and their output signals are sampled by a digital oscilloscope at the rate of 1 GHz.

During measurements, the peak value of a detector's signal is recorded for a fixed delay between the pump and the probe. To improve the signal-to-noise ratio, these measurements are averaged over 20 repeats of the experiment for each selected value of delay. Before each measurement, the sample must be moved to a fresh location by use of the *XYZ* positioner. (To reconstruct the optical transient process in a 10-ns time interval requires a fresh area of the sample of approximately 100 μm $\times$ 300 μm.) To maintain a tight focus on the sample, a module con-

sisting of an astigmatic lens and a four-quadrant detector is used to generate a focus-error signal, which is then fed back to the sample's Z positioner for focus adjustment.

In addition to the pump-and-probe function, our tester is designed to allow *in situ* observation of recorded marks. A white-light source, brought to the bench by a fiber bundle, is used for illumination. The sample's image is picked up by a CCD camera through the microscope objective, beam splitter BS 4, and a focusing lens. (No lens is attached to the camera.)

3. Results and Discussion

Real-time reflectivity and transmissivity measurements were conducted with the pump-and-probe tester on three phase-change samples. Sample 1 was a 25 nm-thick PC layer of $Ge_2Sb_{2.3}Te_5$ (GST) coated onto a fused-silica substrate and protected with a 50 nm-thick SiO_2 layer. Trilayer Sample 2 contained a 75-nm-thick GST layer sandwiched between two ZnS–SiO_2 dielectric layers on a glass substrate. The dielectric layer in contact with the substrate was 120 nm thick, and that coated onto the GST layer was 110 nm thick. Sample 3 was a quadrilayer stack similar to conventional PC recording media; it had a 100-nm Al-alloy layer, a 25-nm ZnS–SiO_2 layer, a 20-nm GST layer, and a 95-nm ZnS–SiO_2 layer coated onto a polycarbonate substrate. These samples were deliberately chosen in experiments for their considerable difference in cooling rates. Before our experiments, the GST layer in all the samples was in the as-deposited amorphous state. We used a static tester to crystallize a 1 mm $\times$ 1 mm area of each sample by slow scanning of a focused laser beam.[10]

In all the experiments reported here the pump beam (as well as the parallel probe beam) was focused onto the PC stack through the sample's substrate; see Fig. 2. To create a large mark, we limited the pump beam at the entrance pupil of the objective by Iris 1 to ~3-mm diameter (see Fig. 1), whereas the probe beam overfilled the lens. (Both objectives had a clear aperture diameter of ~7 mm.) In what follows, a center probe is one that is aligned to coincide with the center of the focused pump spot at the sample, whereas an edge probe falls on the boundary of the molten pool produced by the pump pulse. The threshold pulse power for writing an amorphous mark in the crystallized region was experimentally determined for each sample. During measurements, we set the pump power to be 30–70% greater than the threshold value; no ablation was observed at the pump powers used. The quenched amorphous marks thus recorded had diameters in the range 1.0–1.5 μm. The probe is generally much weaker than the pump, thus preventing complications that might arise from its own thermal effects. Also, the state of polarization of the probe beam is normal to that of pump beam, which mitigates the interference between the two beams, allowing us to have a time resolution better than 510 ps.

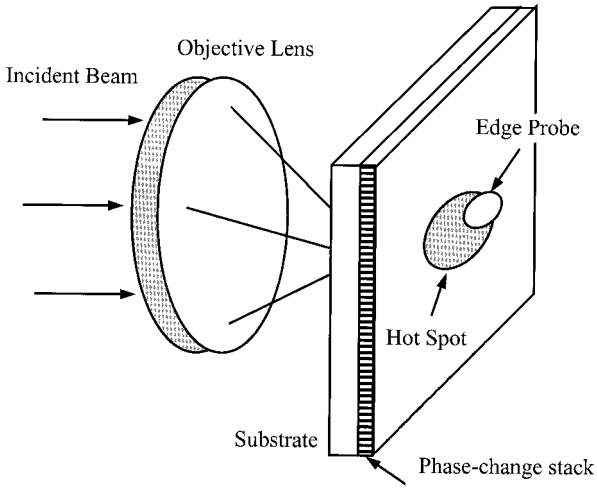

Fig. 2. Pump focused on the PC stack through the sample substrate. The probe may be focused through the same objective, in which case it is referred to as a parallel probe, or through a different objective located on the opposite side of the sample, in which case it is an antiparallel probe. In both cases the probe beam overfills the aperture of the lens, yielding a small focused spot. In contrast, the pump beam may be confined to a small aperture before entering the lens, which results in a larger focused spot at the PC layer. A center probe is one that is aligned to coincide with the center of the focused pump at the sample, whereas an edge probe falls onto the boundary of the molten pool produced by the pump pulse.

A. Amorphization and Recrystallization in a 25-nm-Thick Phase-Change Layer

Figure 3 shows measured transient reflectivity R and transmissivity T as functions of time after irradiation of Sample 1 by a $\tau = 510$ ps, $E = 310$ pJ pump pulse. (The threshold pump energy for forming a visible mark in the PC layer is ~240 pJ.) These measurements were conducted on a precrystallized area of the sample whose R and T values (before exposure to the pump) are given in Fig. 3 at time $t = 0$. Those values of R and T measured in the as-deposited amorphous region are $R = 37\%$ and $T = 16\%$ in a parallel probe. In an antiparallel probe, $R = 34\%$ in the as-deposited amorphous region. Under illumination of a focused beam of light, the local temperature in the sample rises. According to our previous studies, reflectivity changes only slightly with temperature (~1%) unless the PC layer is melted.[11] Because of the similarity in structure between the amorphous state and the molten state, we expect that reflectivity in the molten region will be close to that in the as-deposited region.[12]

We obtained the results shown in Fig. 3(a) by using a parallel, 7-pJ probe pulse. It can be seen that, under irradiation by the pump pulse, R drops rapidly to below 40% while T increases to ~12%; both phenomena are attributed to the melting of the PC layer in the region of the hot spot. Once the pump is turned off, R increases gradually, reaching a maximum after ~5 ns, and then decreases slowly; not surprisingly, the variations of T are in the opposite

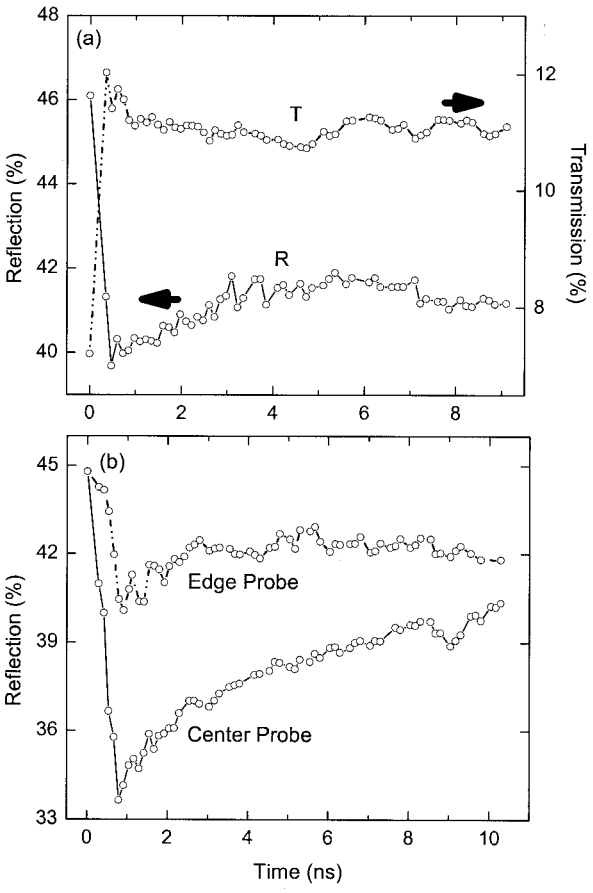

Fig. 3. Transient reflectivity and transmissivity as functions of time, measured on the crystallized area of Sample 1 after irradiation by a $\tau = 510$ ps, $E = 310$ pJ pump pulse arriving at $t = 0$. (a) Both the pump and the (parallel) probe impinge upon the sample through the sample's substrate. (b) The antiparallel probe arrives on the PC layer from the opposite side of the sample. Transient reflectivity curves are shown both for a center probe and for an edge probe.

direction. Solidification of the molten pool followed by slow relaxation is the likely cause of the observed behavior.

Figure 3(b) shows transient reflectivity curves obtained with an antiparallel, 6-pJ probe pulse shining on the back side of Sample 1; all other experimental conditions are the same as those in Fig. 3(a). The bottom curve in Fig. 3(b) is obtained when the focused probe is centered on the written amorphous mark (center probe), and the top curve represents the case when the probe's focused spot is displaced from the center of the mark, falling on the mark's boundary (edge probe). With the center probe, one can observe that R drops rapidly to a minimum immediately after the pump pulse and then rises gradually. Except for a shallow dip near $t = 9$ ns, no decline in R can be observed during the 10.5-ns interval examined. For the edge probe in Fig. 3(b), R drops initially, but the drop is delayed relative to the center probe. Because of the delay, the melting in the edge region is partially due to heat flow from the hottest central region. After this initial drop, the reflectivity measured near the edge of the molten pool increases with a few oscillations and, beyond $t \sim 3$ ns, exhibits only small variations. After $t \sim 6$ ns, the edge region's R begins to decline, albeit slowly. Comparing the results of the edge probe with those of the center probe depicted in Fig. 3(b), one can conclude that the PC layer cools from the edge of the molten pool toward the center and that amorphization is likely to proceed in the same direction.

The reflectivity transient measured in Sample 1 through the substrate and shown in Fig. 3(a) differs considerably from that measured from the film side of the same sample and shown in Fig. 3(b), center probe. The latter rises steadily after the pump pulse, whereas the former increases slowly at first, reaches a peak, and then begins to decline. The PC layer in this sample is coated onto a 1.6-mm-thick fused-silica substrate and protected by a 50-nm-thick layer of SiO_2. Because the thermal conductivity of the substrate, 0.014 (W/cm)/K,[13] is more than twice that of the silica cover layer, 0.006 (W/cm)K,[14] it is conceivable that the PC film's interface with the substrate might have cooled faster than its interface with the cover layer.

B. Amorphization and Recrystallization in a 75-nm-Thick Phase-Change Layer

Before irradiation of the pump pulse, Sample 2 has reflectivity $R = 63\%$ in a crystallized region and 40% in the as-deposited amorphous region for the incidence of light through the substrate (parallel probe). In the antiparallel configuration, $R = 62\%$ in the crystallized region and $R = 43\%$ in the as-deposited amorphous region. Figure 4 shows the reflectivity transients obtained in a precrystallized area of Sample 2 after irradiation of a pump pulse of energy $E = 320$ pJ. Note that in Fig. 4(a) the scale is different for the two curves. The threshold pump power for writing an amorphous mark on this sample is ~230 pJ.

In Fig. 4(a) pump irradiation causes a rapid initial drop in reflectivity, followed by a brief rise and then a subsequent decline of R. The increase of R immediately after melting indicates the onset of a liquid-to-solid phase transition. After ~2 ns, the solid is gradually relaxed to an amorphous phase. A comparison of the reflectivity transients between the center probe and the edge probe in Fig. 4(a) reveals that melting in the edge region begins ~125 ps later than it does in the central region and that the minimum of the R curve is also delayed by ~250 ps. This indicates that the PC layer is initially melted at the center of the focused spot and that the molten pool expands subsequently, in agreement with our observations for Sample 1; see Fig. 3(b). Once irradiation is turned off, the molten pool at the boundary solidifies faster than it does at the center.

The transient reflectance observed from an antiparallel probe, shown in Fig. 4(b), differs substantially from that observed at the substrate interface, where the pump beam is strongly absorbed. Here reflectivity R monitored by the center probe decreases

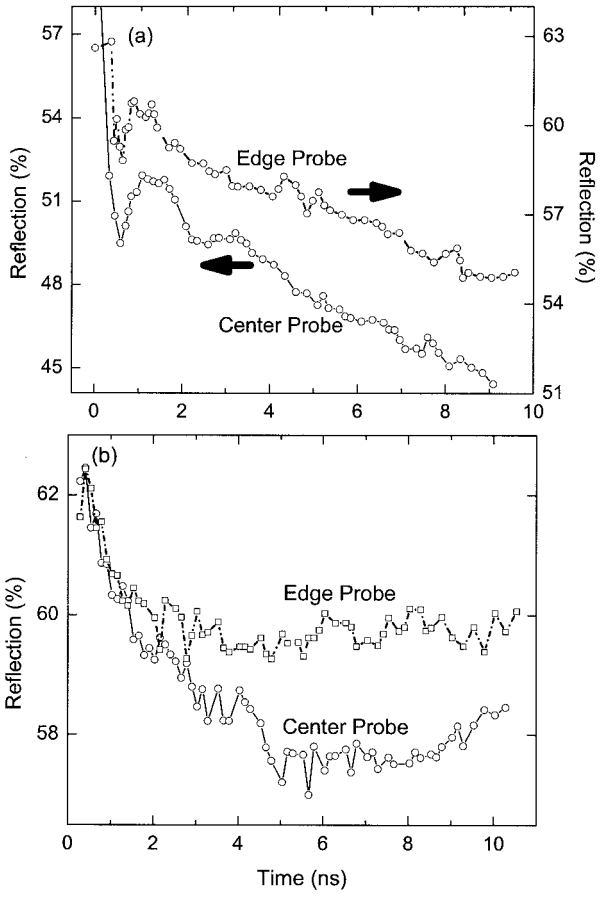

Fig. 4. Transient reflectivity versus time, measured on the crystallized area of Sample 2 after irradiation by a $\tau = 510$ ps, $E = 320$ pJ pump pulse. (a) The pump and the probe are parallel, both arriving on the PC film through the sample's substrate. (b) The antiparallel probe monitors the sample from the surface side. In both cases the edge probe reveals higher levels of reflectivity (and less variation during the transient period) than the center probe.

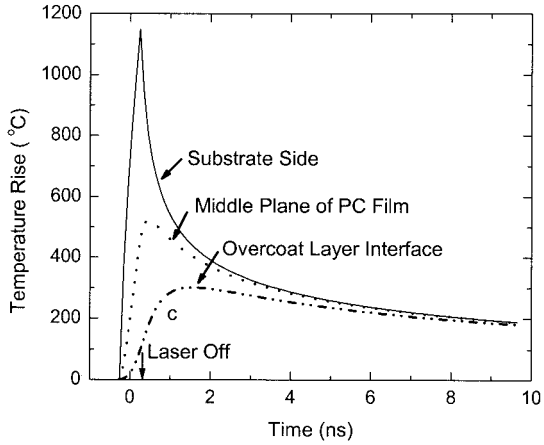

Fig. 5. Computed plots of temperature versus time at the center of the hot spot at various depths through the 75 nm-thick GST film of Sample 2. The solid curve is obtained at the interface of the GST film with the dielectric layer directly deposited onto the substrate, the dotted curve represents the middle plane of the GST film, and the dashed–dotted curve corresponds to the interface between the GST film and the dielectric overcoat. From $t = -255$ ps to $t = +255$ ps the sample is irradiated (through its substrate) with a focused pump beam with $\lambda = 532$ nm, FWHM diameter 1.25 μm, $P = 627$ mW, and $\tau = 510$ ps. The large thickness of the GST film (compared to the skin depth for this material) as well as the different thermal conductivities of the substrate and the dielectric coating layer is responsible for the vastly different temperature profiles through the film thickness. The parameter values assumed in this simulation are as follows: For the glass substrate, the refractive index is $n = 1.5$; the specific heat is $C = 2.0$ J/cm^3/K, and the thermal conductivity is $K = 0.011$ (W/cm)/K. For the ZnS–SiO_2 dielectric layers, $n = 2.14$, $C = 2.0$, and $K = 0.006$. For the GST phase-change layer, $n + ik = 3.2 + i3.8$, $C = 1.285$, and $K = 0.018$.

rather slowly, reaching a minimum after ~5 ns. Beyond $t \sim 8$ ns, R begins to rise gradually. In contrast, R monitored near the edge of the pump beam approaches a steady-state value (with slight oscillations) after $t \sim 3$ ns.

Sample 2 is a trilayer stack consisting of a 75-nm GST layer sandwiched between two dielectric layers. The optical penetration depth into the crystallized PC layer is estimated to be ~22 nm. To understand the different behavior of the reflectance transient in parallel and in antiparallel probes, we calculate the temperature distribution in the sample, using full-vector diffraction theory to compute optical absorption and solving the heat diffusion-equation in three-dimensional space and in time.[5] In the simulation it is assumed that the refractive indices and thermal coefficients of substrate, PC layer, and dielectric layers are temperature independent. Neither the latent heat of the solid-to-liquid phase transition nor the exothermic heat released during solidification is taken into account. Figure 5 shows the computed plots of temperature versus time at the front facet of the PC layer nearest the substrate (solid curve), at the middle plane of the PC layer (dotted curve), and at the rear facet of the PC layer, i.e., at the interface with the protective dielectric layer (dashed–dotted curve). The simulation parameters are listed in the figure's caption.[11] It can be observed that only a thin layer of the PC film, ~25 nm, on the substrate side can actually reach the melting point.

Figure 6 shows the reflectivity transients obtained with a parallel probe on an as-deposited amorphous region of Sample 2. The two curves in this figure correspond to two different pump energies: $E = 240$ pJ for the upper curve and $E = 130$ pJ for the lower curve. These pulse energies are chosen on the basis of the results shown in Fig. 4, accounting for the different absorption coefficients of the amorphous and crystalline phases of the sample. For the lower curve in Fig. 6 the pump is so weak as to preclude any melting of the PC layer. As for the upper curve, the high-energy pump causes a sudden rise in R, from 40% to ~46%. After a few weak oscillations in the vicinity of $t \sim 0.5$ ns, R decreases with time and gradually approaches a final steady-state value. This steady-state value is ~1% greater than the initial reflectivity of the sample, indicating perhaps a

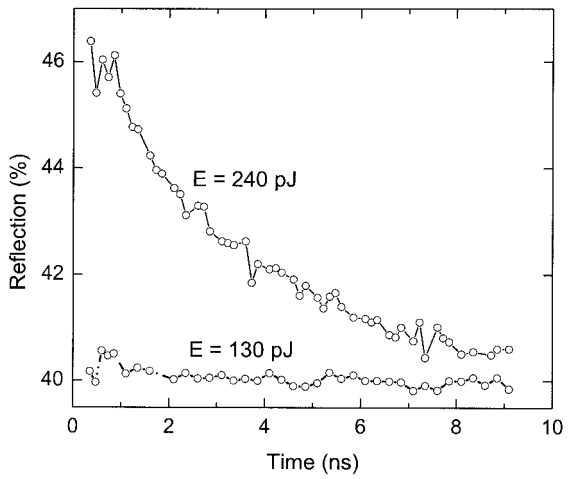

Fig. 6. Transient reflectivity versus time, measured on the as-deposited amorphous region of Sample 2, pumped by $\tau = 510$ ps pulses of different powers. Energy $E = P\tau$ contained in the pump pulses is 240 and 130 pJ. A centered parallel probe monitors the sample in both cases.

slight difference between the melt-quenched and the as-deposited amorphous states. In a comparison of the upper curve of Fig. 6 with the lower curve of Fig. 4(a), it is interesting to note that amorphization takes somewhat longer when one starts from a crystallized region than when the initial state of the sample is amorphous.

C. Amorphization and Recrystallization in a Rapid-Cooling Structure

Before exposure of the pump pulse, Sample 3 has reflectivity $R = 40\%$ in the crystallized region and 10.6% in the as-deposited amorphous region. Figure 7 shows the reflectivity transients obtained from a precrystallized region of Sample 3 by use of a parallel probe. The lower curve corresponds to a center probe, and the upper curve represents an edge probe. Pump pulse energy $E = 260$ pJ is ~73% greater than the threshold pulse energy of ~150 pJ required for amorphization in this case.

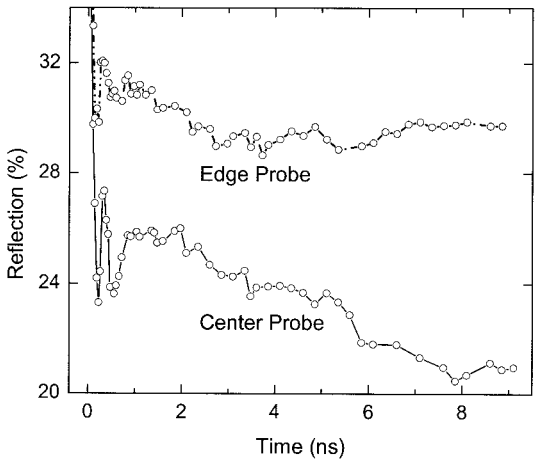

Fig. 7. Transient reflectivity versus time, measured on the crystallized area of Sample 3 after irradiation by a $\tau = 510$ ps, $E = 260$ pJ pump pulse. Both the pump and the probe arrive on the PC film through the sample's substrate. The edge probe reveals higher reflectance (and less variation during the transient period) than the center probe.

Once again, the pump irradiation melts the PC layer and causes R to drop from 40% to 23%. Interestingly, following the drop, R suddenly increases and then decreases again. This change of R by as much as 4% can be seen in the lower curve in Fig. 7. The same phenomenon was also observed in Samples 1 and 2, although the change in R in those instances was not so pronounced. To our knowledge, such an ultrafast phenomenon has never been reported in the literature.

Sample 3 is a quadrilayer stack that has an Al-alloy layer as a reflector as well as a heat sink. The thermoelastic property of the Al alloy is quite different from that of the dielectric layer. During irradiation by a subnanosecond focused beam, the absorbed light in the PC layer causes submicrometer-sized local heating and causes transient thermal expansion and high elastic stress in the film.[14] The fast solid-to-liquid phase transition causes a sudden decrease in the volume of the PC layer. The thermoelastic mechanism is suppressed by homogeneous melting across the PC layer. The time interval between the two minima of the spike in Fig. 7 is related to the time needed for complete melting of the PC layer through thermal diffusion. That diffusion time is estimated to be ~250 ps, which is close to the ~340-ps interval between the two minima.

Once the laser pulse is turned off, the molten pool cools and solidifies. The structural phase transition from liquid to solid results in a rapid increase of R. Following solidification, the molten spot relaxes slowly to the amorphous state and R decreases, similarly to what was observed for Samples 1 and 2; see Figs. 3(a) and 4(a). In particular, the reflectivity of the liquid phase is significantly higher than that of the amorphous phase at room temperature.

A comparison of the R transients of Sample 3 obtained with the center probe and with the edge probe indicates that cooling of the molten pool proceeds from the boundary to the center, which is also the way in which amorphization proceeds in this sample. Amorphization is frustrated by growth of the crystalline phase from the boundary, which is indicated by the rise in R from the edge probe after $t \sim 5$ ns.

Figure 8 shows the R transients observed in an as-deposited amorphous region of Sample 3 on irradiation by a pump pulse. The pulse energy for the top curve, which shows the effects of localized melting of the PC layer, is $E = 180$ pJ, and that for the bottom curve, which is intended not to melt the PC layer at all, is $E = 90$ pJ. When the pump fluence is low, R increases initially by ~1.5% and subsequently reaches a steady state after ~1 ns. At high fluence, however, R jumps abruptly from 10.6% to 18.2% and subsequently declines to a stable final value that is

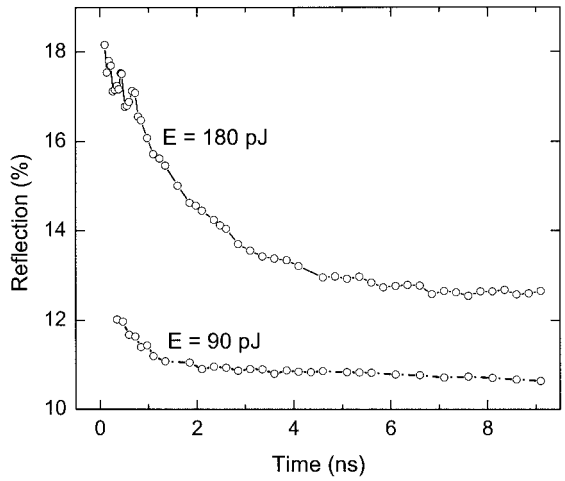

Fig. 8. Transient reflectivity versus time, measured on the as-deposited amorphous region of Sample 3, pumped by $\tau = 510$ ps pulses of different powers. Energy $E = P\tau$ contained in the pump pulse is 180 and 90 pJ. A centered parallel probe monitors the sample in both cases.

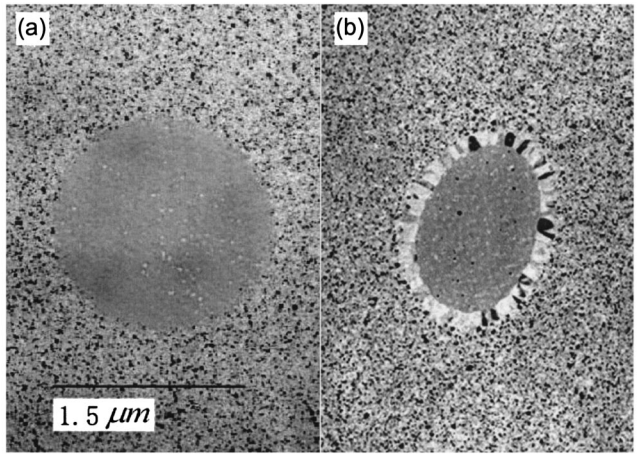

Fig. 9. Transmission electron microscope images of amorphous marks written on Sample 3 by pulses of (a) $\tau = 510$ ps duration and (b) 500-ns duration.

~2% greater than the initial reflectivity of the sample. Under the microscope there appears a faint contrast between the exposed area and its surroundings, confirming perhaps the partial crystallization of the molten pool during cooldown. Weak oscillations can be observed in the R transient right immediately after irradiation with the high-power pump pulse. Consistent with our observation for Sample 2, the relaxation time for amorphization starting from the sample in its crystalline state is somewhat longer than that from the sample in its amorphous state (compare the lower curve in Fig. 7 with the upper curve in Fig. 8).

A comparison of Figs. 6 and 8 reveals that, owing to the high thermal conductivity of the Al-alloy layer, Sample 3 cools faster than Sample 2; nonetheless, partial crystallization during cooldown from the melt is observed in both samples.

One consequence of short-pulse recording, which was also noted previously,[6] is the formation of a sharp, clean boundary between the recorded amorphous mark and its surrounding crystalline environment. Figure 9 shows transmission electron microscope images of amorphous marks written on Sample 3. In Fig. 9(a) the mark was written with a $\tau = 510$ ps pulse; in Fig. 9(b) the mark was written with a fairly long ($\tau = 500$ ns) laser pulse. Note the appearance in Fig. 9(b) of a ring containing relatively large crystallites, which are formed during slow cooling at the edge of the molten pool; rapid cooling [Fig. 9(a)] prevents the formation of the ring.

4. Concluding Remarks

Using transient reflectivity measurements with a pump-and-probe technique, we investigated the amorphization dynamics of several phase-change samples of different layer structures. Amorphization triggered by subnanosecond laser pulses was achieved in all the samples. This study indicates that amorphization involves rapid melting, liquid-to-solid phase transition, and subsequent structural relaxation. Partial crystallization during amorphization was also observed in these samples.

The authors are grateful to J. Kevin Erwin, Warren Bletscher, and Xiaodong Xun of the Optical Sciences Center, University of Arizona, for their technical support. Sample 1 was prepared by Lynda Busse of the U.S. Naval Research Laboratory, and Samples 2 and 3 were fabricated at Matsushita Electric Industries of Japan by Kenichi Nagata and Takeo Ohta. The transmission electron micrographs in Fig. 5 were supplied by Byung-ki Cheong of the Korea Institute of Science and Technology. This research has been sponsored by the Optical Data Storage Center of the University of Arizona.

References

1. J. Feinleib, J. de Nuefville, S. C. Moss, and S. R. Ovshinsky, "Rapid reversible light-induced crystallization of amorphous semiconductors," Appl. Phys. Lett. **18,** 254–257 (1971).
2. D. J. Gravesteijn, "Materials developments for write-once and erasable phase-change optical recording," Appl. Opt. **27,** 736–738 (1988).
3. T. Ohta, K. Inoue, M. Uchida, K. Yoshioka, T. Akiyama, S. Furukawa, K. Nagata, and S. Nakamura, "Phase-change disk media having rapid cooling structure," Jpn. J. Appl. Phys. **28,** Suppl. **28-3,** 123–128 (1989).
4. K. A. Rubin and M. Chen, "Progress and issues of phase-change erasable optical recording media," Thin Solid Films, **181,** 129–139 (1989).
5. C. Peng, L. Cheng, and M. Mansuripur, "Experimental and theoretical investigations of laser-induced crystallization and amorphization in phase-change optical recording media," J. Appl. Phys. **82,** 4183–4191 (1997).
6. T. Ohta, N. Yamada, H. Yamamoto, T. Mitsuyu, T. Kozaki, J. Qiu, and K. Hirao, "Progress of the phase-change optical disk memory," in *Applications of Ferromagnetic and Optical Materials, Storage and Magnetoelectronics*, Vol. 674 of Materials Research Society Proceedings, M. Wuttig, L. Hesselink,

and H. J. Borg, eds. (Materials Research Society, Warrendale, Pa., 2001), pp. V1.1.1–12.
7. C. N. Afonso, J. Solis, and F. Catalina, "Ultrafast reversible phase change in GeSb films for erasable optical storage," Appl. Phys. Lett. **60,** 3123–3125 (1992).
8. J. Siegel, C. N. Afonso, and J. Solis, "Dynamics of ultrafast reversible phase transitions in GeSb films," Appl. Phys. Lett. **75,** 3102–3104 (1999).
9. J. U. White, "Long optical paths of large aperture," J. Opt. Soc. Am. **32,** 285–288 (1942).
10. M. Mansuripur, J. K. Erwin, W. Bletscher, P. Khulbe, K. Sadeghi, X. Xun, A. Gupta, and S. B. Mendes, "Static tester for characterization of phase-change, dye-polymer, and magneto-optical media for optical data storage," Appl. Opt. **38,** 7095–7104 (1999).
11. G. Peng and M. Mansuripur, "Measurement of the thermal coefficients of rewritable phase-change optical recording media," Appl. Opt. **41,** 361–369 (2002).
12. M. Ono, K. Yasuda, A. Fukumoto, and M. Kaneko, "A high density read-only optical disk system using superresolution and an SHG green laser," in *Optical Data Storage '95*, G. R. Knight, H. Ooki, and Y.-S. Tyan, eds., Proc. SPIE **2514,** 20–27 (1995).
13. R. Frank, V. Drach, and J. Fricke, "Determination of thermal conductivity and specific heat by a combined 3ω/decay technique," Rev. Sci. Instrum. **64,** 760–765 (1993).
14. A. J. Griffin, F. R. Brotzen, and P. J. Loos, "Effect of thickness on the transverse thermal conductivity of thin dielectric films," J. Appl. Phys. **75,** 3761–3764 (1994).